THE JOURNAL OF BIOLOGICAL CHEMISTRY VOL. 281, NO. 36, pp. 25972–25983, September 8, 2006

Allosteric Effectors Influence the Tetramer Stability of Both R- and T-states of Hemoglobin A*

Received for publication, May 2, 2006, and in revised form, June 23, 2006 Published, JBC Papers in Press, July 5, 2006, DOI 10.1074/jbc.M604216200

Gusztáv Schay[‡], László Smeller[‡], Antonio Tsuneshige[§], Takashi Yonetani[§], and Judit Fidy[‡1]

From the [‡]Department of Biophysics and Radiation Biology and Biophysics Research Group of the Hungarian Academy of Sciences, Faculty of Medicine, Semmelweis University, P. O. Box 263 H 1444 Budapest, Hungary and the [§]Department of Biochemistry and Biophysics, University of Pennsylvania School of Medicine and the Johnson Research Foundation, Philadelphia, Pennsylvania 19104-6059

The contribution of heterotropic effectors to hemoglobin allostery is still not completely understood. With the recently proposed global allostery model, this question acquires crucial significance, because it relates tertiary conformational changes to effector binding in both the R- and T-states. In this context, an important question is how far the induced conformational changes propagate from the binding site(s) of the allosteric effectors. We present a study in which we monitored the interdimeric interface when the effectors such as Cl^-, 2,3-diphosphoglycerate, inositol hexaphosphate, and bezafibrate were bound. We studied oxy-Hb and a hybrid form $(\alpha FeO_2)_2$-$(\beta Zn)_2$ as the T-state analogue by monitoring heme absorption and Trp intrinsic fluorescence under hydrostatic pressure. We observed a pressure-dependent change in the intrinsic fluorescence, which we attribute to a pressure-induced tetramer to dimer transition with characteristic pressures in the 70–200-megapascal range. The transition is sensitive to the binding of allosteric effectors. We fitted the data with a simple model for the tetramer-dimer transition and determined the dissociation constants at atmospheric pressure. In the R-state, we observed a stabilizing effect by the allosteric effectors, although in the T-analogue a stronger destabilizing effect was seen. The order of efficiency was the same in both states, but with the opposite trend as inositol hexaphosphate > 2,3-diphosphoglycerate > Cl^-. We detected intrinsic fluorescence from bound bezafibrate that introduced uncertainty in the comparison with other effectors. The results support the global allostery model by showing that conformational changes propagate from the effector binding site to the interdimeric interfaces in both quaternary states.

Hemoglobin (1) is a tetrameric protein, which plays a vital role in the transport of oxygen. It consists of two dimers of α and β subunits that reversibly bind and release oxygen (1). The description of this cooperative phenomenon has been most frequently derived from the Monod-Wyman-Changeux (MWC)[2] two-state allosteric model (2) that attributes cooperativity to a rapid equilibrium between two conformations of distinct oxygen affinity of the whole tetramer. These distinct states are the fully unliganded T-state and the fully ligated R-state. Szabo and Karplus (3) modified the two-state model incorporating the stereochemical mechanism suggested by Perutz (4) for the T to R switch, and introduced ligation-induced tertiary changes within the T-state. In this extended model (MWC-SK), it was proposed that cooperativity still works through a ligation-induced shift in the equilibrium of states T and R, but the model attributed importance in the conformational switch to certain changes at the inter- and intrasubunit interfaces. Upon ligation in the T-state, the network of intersubunit interactions become perturbed, some (*e.g.* salt bridges) become broken up to release the characteristic strain of the T-state. The mechanism involves a rotation of one dimer with respect to the other, thus reaching the more relaxed R-state (5).

It has been widely reported that some molecules, referred to as heterotropic allosteric effectors, considerably lower the oxygen affinity of the T-state upon binding to HbA but not to the heme (6–9). Structural studies in the T-state showed that these allosteric effectors primarily bind to the central cavity of HbA (10–12). The modulation of the oxygen dissociation curves by allosteric effectors is addressed in the extended MWC model by the assumption that allosteric effectors bind specifically to the somewhat larger central cavity of the T-state and stabilize this conformation. This shifts the R/T equilibrium in favor of the T-state and consequently lowers the overall affinity to oxygen (8, 13). The well known Bohr effect and results reported for Cl^-, also influencing the oxygen affinity of the T-state (14, 15), show that, in a broader sense, H^+ and Cl^- can also be considered as being members of the family of allosteric effectors.

Extended studies on the effect of allosteric effectors, however, indicated that they not only bind to the T-state but also to the R-state (16, 17). The modulation of the oxygen association constants was shown to occur at a much broader scale (65-fold change in K_T and 2000-fold change in K_R; see Ref. 18 for details)

* This work was supported by a collaborative grant from the Fogarty International Center, Award TW005924 (to T. Y. and J. F.), National Science Foundation of Hungary Grants OTKA T049213 (to L. S.) and OTKA TS-044730 (to J. F.), by NHLBI Grant HL14508 from the National Institutes of Health (to T. Y.), and by a Ph.D. fellowship from Eötvös University, Budapest (to J. F.). The costs of publication of this article were defrayed in part by the payment of page charges. This article must therefore be hereby marked "*advertisement*" in accordance with 18 U.S.C. Section 1734 solely to indicate this fact.

[1] To whom correspondence should be addressed. Fax: 36-1-2666656; E-mail: judit@puskin.sote.hu.

[2] The abbreviations used are: MWC, the two-state allosteric model of Monod; Wynan, and Changeaux; HbA, human adult hemoglobin; oxy-Hb, native human adult hemoglobin A linked to oxygen; α-oxy-Fe-βZn-Hb, zinc-substituted $\alpha(FeO_2)_2$-$\beta(Zn)_2$ human hemoglobin; Zn-PP-IX, zinc-protoporphyrin-IX; IHP, inositol hexaphosphate; BZF, bezafibrate; DPG, 2,3-diphosphoglycerate; MPa, megapascal; GPa, gigapascal; FTIR, Fourier transform infrared spectroscopy.

in each state than previously known. These data initiated the reformulation of the earlier models for the allosteric action of heterotropic effectors. The recently proposed "global allostery model" (18) supposes that the effectors can bind to both the T- and R-states and that effectors induce direct tertiary conformational changes. These tertiary effects then lead to the detected changes in oxygen association (18, 19). Until now, no structural data have been published for the complex of R-state human HbA with allosteric effectors; the only available structure is that of horse HbA complexed to CO (20). Recently, however, a docking and molecular dynamics simulation study in our laboratory (21) proposed models for the structure of HbA bound with the allosteric effectors DPG, IHP, and 2-{4-{(3,5-dichlorophenylcarbamoyl)-{methyl}-phenoxy}-2-methylpropionoc acid. These results supported the model allowing for binding of effectors also in the R-state and proposed primary binding sites in the central cavity of the R-state tetramer.

In this paper we report the results of high pressure studies. We show that pressure perturbation of the structure is a valuable tool providing the means to measure the tetramer-dimer dissociation constant. This parameter reports structural changes at the interdimeric interface.

High pressure is known to have distinct effects on proteins (22) depending on the applied pressure range. Typically, 0.5–1 GPa is needed to denature a protein, by squeezing water into the interior (23). Lower pressure causes elastic deformations, the extent of which are characteristic of the compressibility (24, 25) of the protein. Because pressure is a thermodynamic parameter, pressure can shift thermodynamic equilibria of various kinds, including conformational transitions of proteins (26). One such equilibrium that is typically perturbed by pressure is oligomer dissociation. Pressures in the range of 100–200 MPa have been shown to be able to affect the quaternary structure of the proteins without affecting their secondary and tertiary structure (27). Previous pressure experiments performed on HbA (28–30) showed that pressure tuning affects various optical properties (*e.g.* light scattering, absorption, fluorescence emission, and CD spectra) of the sample. In a detailed study, Pin *et al.* (28) showed that applying pressure at pH 7 and 10^{-6}–10^{-4} M protein concentration will shift the tetramer-dimer equilibrium in favor of the dimers, and at pH 9, the observed dimer-monomer equilibrium will be shifted in favor of the monomers. Although Pin *et al.* (28) included IHP in their study, no systematic study applying pressure perturbation was conducted to observe the effect of various allosteric effectors on the subunit interfaces in HbA.

In this study our goal was to compare the effect of allosteric effectors on the tetramer-dimer equilibrium in the T- and R-states by applying high hydrostatic pressure and steady-state fluorescence techniques. Based on literature data (31, 32), we have used the intrinsic fluorescence of the tryptophan residues as a marker of changes at the interface region. Measurements under high hydrostatic pressure were, however, not feasible on deoxyhemoglobin, because the sample holder inside the pressure cell cannot be isolated in a gas-tight manner from the pressure transmitter fluid (water) in the device. To overcome this difficulty, we used a hybrid hemoglobin, α-oxy-Fe-βZn-Hb to mimic the structure of the T-state. In this hybrid the hemes of the β subunit are replaced with Zn-protoporphyrin-IX, and the α-subunit hemes are oxygen-ligated. Oxygen equilibrium studies and x-ray crystallography have shown that this derivative, as a five-coordinated metal hybrid of HbA, can be considered analogous to T-state HbA (33–35).

The selection of zinc substitution is supported by results that show a low energetic cost compared with other (for *e.g.* cobalt) metal substitutions (36). This indicates that the conformation is close to the native form. It can be considered questionable, however, for which of the T-state subpopulations the analogy holds. The conformation within being "T" was shown to be slightly tunable by environmental conditions, for example by sol-gel encapsulation (37, 38). This tunability was also found within zinc hybrids rendering the CO-ligated form the least tense among a variety of ligated forms and external conditions (39). Literature data, however, show that the zinc hybrids in general have lower oxygen affinity than deoxy-HbA (40). Based on this we considered the $(\alpha FeO_2)_2$-$(\beta Zn)_2$ form, which may be the least tense among the zinc hybrids, a sufficiently good model for the native T-state under physiological conditions. We used the oxy-form of HbA to study the R-state.

The effect of the allosteric effectors Cl^-, IHP, DPG, and BZF was investigated at pH 7.4 by pressure stability measurements based on the sensitivity of tryptophan fluorescence to structural changes of HbA. We observe a structural transition of the protein in the range of 100–200 MPa, and we argue for this being a tetramer-dimer transition. We show that the characteristic pressure of this transition, and thus the equilibrium constant (K_{d0}) of the reaction, is sensitive to the presence of allosteric effectors both in the R- and in the T-analogue state of HbA. These data characterize the dimer interface of the tetramer that was shown to play a decisive role in the cooperativity of oxygen binding. The reliability of the methodology was confirmed by parallel experiments with horse heart oxy-myoglobin.

EXPERIMENTAL PROCEDURES

Materials—Myoglobin (horse heart), sodium chloride, HEPES, IHP, DPG, and BZF, the highest purity available, were purchased from Sigma.

All samples (both myoglobin and HbA) were prepared in 100 mM HEPES, pH 7.4, with deionized water. IHP and DPG was used in a final concentration of 2 mM, BZF at 10 mM, and the sodium chloride concentration was 100 mM. The IHP, DPG, and BZF concentrations were selected as described previously (19), and these concentrations are well in excess of the 0.06 mM HbA concentration used in the comparative experiments thus ensuring the saturation of the binding sites. Myoglobin was used only in the oxygen-saturated form.

Hemoglobin Preparation—HbA was prepared from human blood as described previously (19) according to the method of Drabkin (41). HbA was promptly converted to the CO form and stripped of organic phosphates by the method of Berman *et al.* (42), and further purified by ion exchange chromatography. The final HbA solution was eluted in 5 mM HEPES buffer, pH 7.4. The native oxygenated HbA samples are referred to as oxy-Hb, and these were obtained from the CO form by strong illumination and a flow of pure oxygen above the sample, which was kept on ice. Zinc-substituted HbA was prepared from

human HbA as described previously (43). The α and β subunits were isolated from CO HbA, and the β subunit was converted to apoprotein by the acid-acetone method and then incubated with Zn-PP-IX to create β-zinc subunits. Finally, the α-Fe and β-zinc subunits were mixed and incubated in the cold for 2 days. The $(\alpha Fe\text{-}CO)_2\text{-}(\beta\text{-}Zn)_2$ form was then converted to the oxy form as described above. The $(\alpha FeO_2)_2\text{-}(\beta Zn)_2$-hemoglobin hybrid is referred to as α-oxy-Fe-βZn-Hb in this paper.

All samples were adjusted to 60 μM final heme concentration before measurement, unless stated otherwise (for concentration dependence measurements). The stripped forms (containing no organic phosphates or Cl^-) were used as reference in all measurements.

Possible denaturation or deoxygenation during experiments was controlled by recording the absorption spectrum. No significant changes were detected in the 270–700 nm wavelength range upon the addition of various effectors or upon increasing the pressure.

Fluorescence Emission Spectra under High Pressure—A high pressure cell with sapphire windows (Unipress, Warsaw, Poland) was mounted in a Fluorolog-3 (Yobin Ivon Inc. Lonjumeau, France) spectrofluorometer. High pressure was created by a manually driven pump (Nova Swiss, Effretikon, Switzerland), and pressure was monitored with a pressure transducer (DMS-580.4018 Nova Swiss, Effretikon, Switzerland) equipped with a digital meter, with an accuracy of 10 bar. The sample was allowed to equilibrate at each pressure for 3 min. Spectra were acquired by integrating for 1 s at each wavelength, with slits adjusted at 5 nm excitation and 2 nm emission bandpass. The spectrofluorometer was equipped with a 450-watt xenon lamp (Osram, München, Germany) as light source. The temperature was maintained by a thermostat at 20 °C and was directly controlled in the sample.

The HbA sample was injected into a quartz tube (UV-fused silica) with a 2.4-mm inner diameter with 1.3-mm wall thickness and 19-mm height. The sample volume was 110 μl. This tube was covered with a rubber stopper and placed into the pressure cell. The pressure transmitter fluid was water.

Spectral shift under pressurization was determined based on either the maximum position of the emission band determined by a Savitzky-Golay algorithm or the center of gravity of the band in the 300–400-nm range. Both kinds of evaluation lead to the same information. We report data based on the maximum positions.

Absorption Spectra at High Pressure—The high pressure cell was mounted in a Cary 4E UV-visible spectrophotometer (Varian Inc, Palo Alto, CA) and kept at 20 °C. Spectra were acquired at a scan rate of 1 nm/s, using the full height slit mode, allowing for 1 nm bandpass. Control spectra before pressurization were acquired in the quartz tube, covered with a rubber stopper, and placed centered in the light beam.

FTIR Spectroscopy Under Pressure—The infrared spectra were obtained with a Bruker IFS66 FTIR spectrometer equipped with a broad band MCT solid-state detector cooled with liquid nitrogen. During data acquisition, 256 interferograms were co-added at a resolution of 2 cm^{-1}. High pressure was generated in a diamond anvil cell (Diacell Products, Leicester, UK), where the pressure was built up by means of a screw

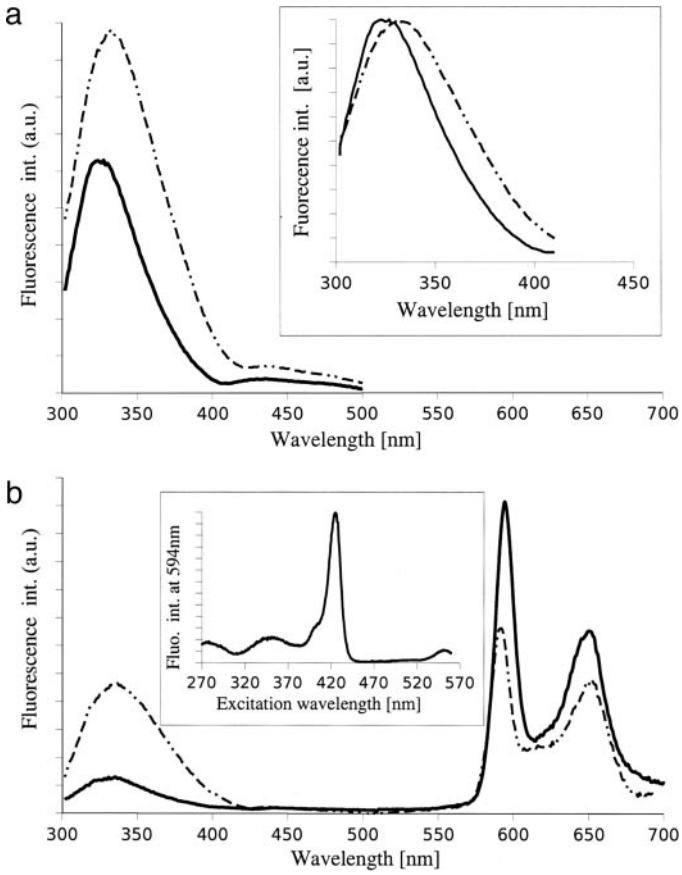

FIGURE 1. **Fluorescence emission spectra excited at 290 nm taken at ambient pressure (*solid lines*) and at 350-MPa hydrostatic pressure (*dashed lines*).** *a*, oxy-Hb; *b*, α-oxy-Fe-βZn-Hb. *Inset* in *a*, normalized spectra of oxy-Hb. *Inset* in *b*, excitation spectrum registered at 594 nm for porphyrin emission. *a.u.*, arbitrary units.

mechanism. Barium sulfate was used as an internal pressure standard in all cases (44). All experiments were performed at 25 °C. The broad band of water around 3350 cm^{-1} was used to control that the solvent is still in the fluid phase even at the highest pressure used in the experiments. No crystallization was observed in the experiments reported here. The overlapping components of the amide I/I′ band were resolved by Fourier self-deconvolution (45), which decreases the width of the component lines of the amide band. The optimal parameters were determined from the analysis of the power spectrum (46). A resolution enhancement factor (45) of 1.5 was reached by using a Lorentzian band shape of 20 cm^{-1} bandwidth. The deconvoluted spectra were then fitted with gaussian functions, and the peak position of the band characteristic for α-helical structure was determined.

RESULTS

Oxy-Hb and α-oxy-Fe-βZn-Hb samples corresponding to the R- and T-analogue state HbA, respectively, were studied in stripped condition as reference and then bound to various allosteric effectors. The effect of allosteric effectors was monitored by registering the conformational perturbation effect of high pressure using fluorescence and absorption spectroscopy.

Effects Shown by Tryptophan Fluorescence—In Fig. 1, the *solid lines* show the fluorescence emission spectra of stripped

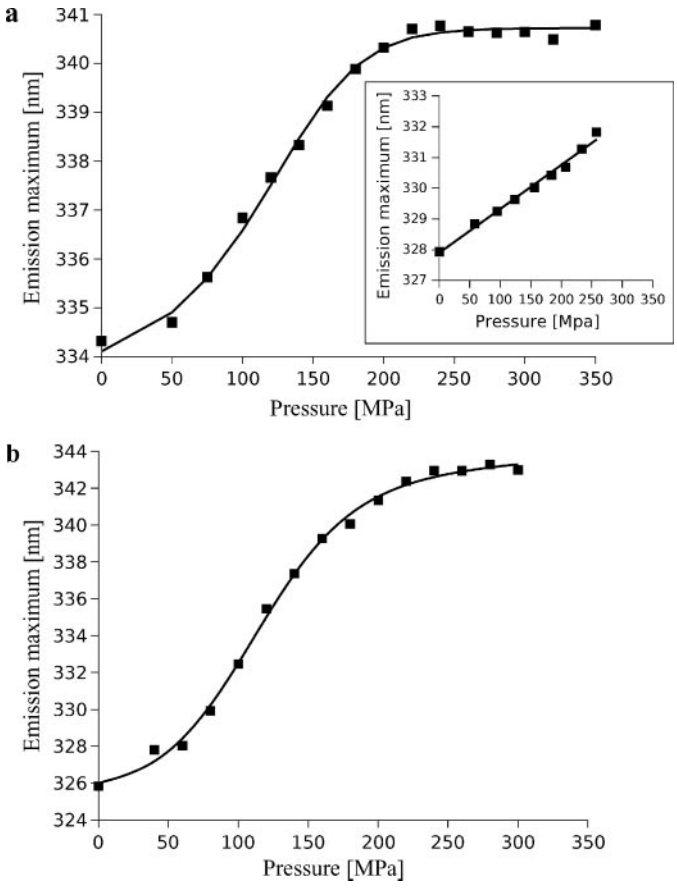

FIGURE 2. **Tryptophan emission maximum position *versus* pressure.** *a,* oxy-Hb with 100 mM chloride. *Inset* shows data for myoglobin; *solid line* is a linear fit to the data. *b,* α-oxy-Fe-βZn-Hb with 100 mM chloride. *Solid line* is a fit of Equation 6 to the data.

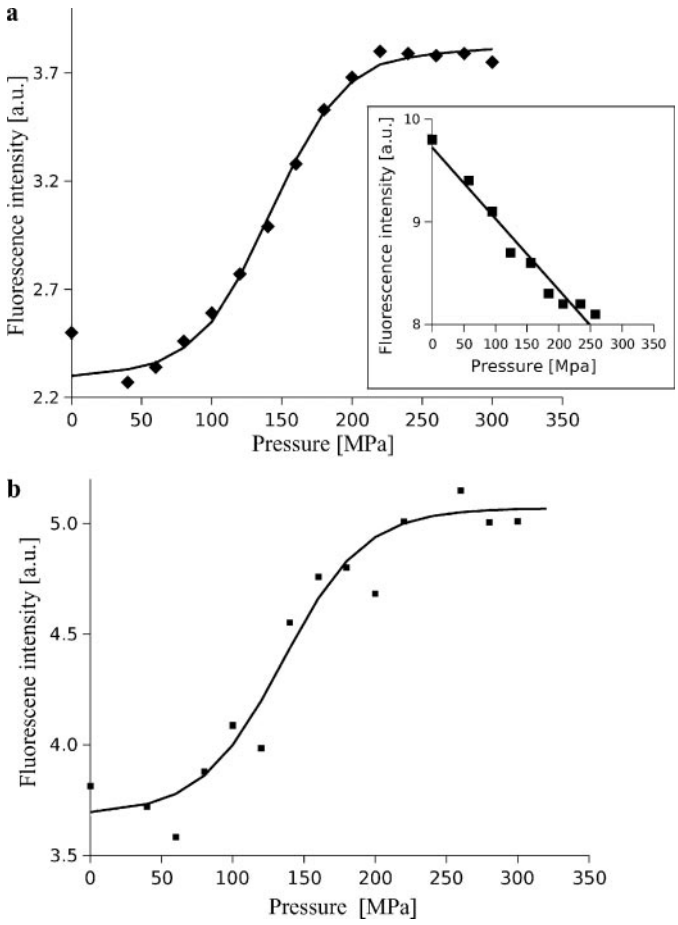

FIGURE 3. **Tryptophan fluorescence intensity at the tryptophan emission maximum *versus* hydrostatic pressure.** *Continuous line* represents a sigmoid fit to the data. *a,* oxy-Hb with 100 mM chloride; $p_{1/2}$ is 142 MPa. *Inset* shows data for myoglobin; *solid line* is a linear fit to the data. *b,* α-oxy-Fe-βZn-Hb with 100 mM chloride; $p_{1/2}$ is 151 MPa. The increased experimental error is because of the increased energy transfer from the Trps to the Zn-PP-IX. *a.u.*, arbitrary units.

oxy-Hb (*a*) and α-oxy-Fe-βZn-Hb (*b*) at ambient pressure; the *dashed lines* are spectra at a pressure of 350 MPa. The excitation wavelength was 290 nm for both samples to directly excite the Trp residues. It is seen that the intrinsic Trp fluorescence is easily measured under the experimental conditions, and a pressure effect can be observed. In the case of oxy-Hb, the emission peak characteristic for the Trp fluorescence can be observed around 330–340 nm, as seen in Fig. 1*a*. For α-oxy-Fe-βZn-Hb (Fig. 1*b*), characteristic Zn-PP-IX emission peaks also appear at 594 and 645 nm, indicative of energy transfer from Trp to the Zn-PP-IX. This is also seen in Fig. 1*b, inset,* where it is directly shown that Zn-PP-IX fluorescence can be excited by Trp absorption. Energy transfer from Trps to the hemes can also be considered in the case of oxy-Hb. A proof for this is a slight dip in the emission spectrum (Fig. 1*a*) around the wavelength of the Soret maximum (~420 nm).

It can be seen that increased pressure induces a red shift (*cf.* Fig. 1*a, inset*), broadening of the Trp fluorescence emission band, and a significant increase of emission intensity.

The red shift of the Trp emission *versus* pressure has a sigmoidal character in all kinds of Hb samples. Fig. 2 shows the maximum positions of the emission peaks *versus* pressure in both quaternary states in the presence of 100 mM chloride. The fluorescence intensity showed the same feature when plotted as a function of increasing pressure (Fig. 3). Both kinds of evaluations lead to a feature that is indicative of a pressure-induced conformational transition. The pressure at 50% transition of a specific sample is very similar when determined from the maximum position or from the increase of quantum yield of Trp emission. In the comparative analysis of the effect of allosteric effectors, we used the data obtained from the red shift of the maximum position. Table 1 shows that the characteristic pressures were sensitive to the presence of bound allosteric effectors in both quaternary states. For comparison we used the data obtained at 60 μM concentration.

Pressure-induced Changes in Tryptophan Fluorescence of Myoglobin—To assess pressure-induced changes at the monomeric level, we report fluorescence data for myoglobin, which has a structure similar to a Hb monomer. The results are shown in the *insets* of the figures reporting data for HbA. Fig. 2*a* and Fig. 3*a, insets,* show the maximum position and the intensity of the Trp emission maximum of myoglobin in the function of pressure, respectively. In contrast to HbA, myoglobin shows a different behavior. The shift of the maximum position is relatively small (few nm/100 MPa) and is strictly linear. The intensity linearly decreases with increasing pressure, in contrast to the sigmoidal intensity increase observed in HbA (Fig. 2*a*).

TABLE 1

$p_{1/2}$ data under various conditions

HbA type indicates the quaternary state, oxyHb or α-oxyFe-βZn-Hb. Stripped, without allosteric effectors. Uncertainty in the $p_{½}$ values are typically in the range of 5–10 MPa.

HbA type	Concentration	Effector	$p_{½}$
	mM		*MPa*
α-Oxy-Fe-βZn-Hb	0.68	None (stripped)	200
α-Oxy-Fe-βZn-Hb	0.23	None (stripped)	160
α-Oxy-Fe-βZn-Hb	0.02	None (stripped)	135
α-Oxy-Fe-βZn-Hb	0.06	None (stripped)	140
α-Oxy-Fe-βZn-Hb	0.06	100 mM Cl^-	113
α-Oxy-Fe-βZn-Hb	0.06	2 mM DPG	95
α-Oxy-Fe-βZn-Hb	0.06	2 mM IHP	72
α-Oxy-Fe-βZn-Hb	0.06	10 mM BZF	165
Oxy-Hb	7.7	None (stripped)	225
Oxy-Hb	0.77	None (stripped)	157
Oxy-Hb	0.06	None (stripped)	100
Oxy-Hb	0.06	100 mM Cl^-	137
Oxy-Hb	0.06	2 mM IHP	144
Oxy-Hb	0.06	10 mM BZF	170

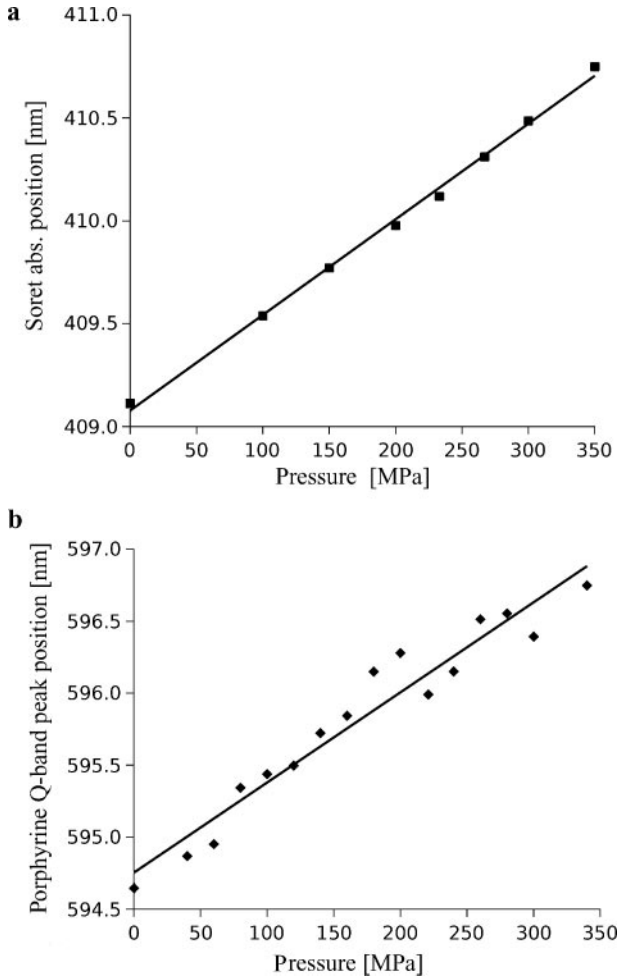

FIGURE 4. *a,* Soret absorption peak maximum position *versus* pressure of stripped oxy-Hb. *Solid line* is a linear fit to the data, with a slope of 4.7 nm/Gpa. *b,* zinc-PP-IX fluorescence emission peak maximum position *versus* pressure (excited at 290 nm) of α-oxy-Fe-βZn-Hb with chloride. *Solid line* is a linear fit to the data; the slope is 6.1 nm/GPa.

Pressure Effect on the Porphyrin Spectra—The electronic transition energy of the porphyrin, monitored either by fluorescence of α-oxy-Fe-βZn-Hb or by the absorption spectra of oxy-Hb, did not show a structural transition upon applying high pressure, unlike that of the Trps. A linear dependence of the maximum position could be measured in the function of increasing pressure up to 350 MPa as shown in Fig. 4. Both the Soret band position in the absorption spectrum of oxy-Hb seen in Fig. 4*a* and the Q-band position in the fluorescence spectrum of α-oxy-Fe-βZn-Hb seen in Fig. 4*b* show a linear dependence. Similarly, linear shifting effects of pressure were observed in all samples. This observation corresponds to the finding of others in the case of cytochromes (47), where a linear shift was also observed in a similar pressure range. It was concluded that in this pressure range the heme pocket of hemoproteins is affected only by elastic deformations resulting in a linear (red) shift of the electronic transition energy. In our experiments the peak positions and the linear shifting effect were not significantly influenced by binding of allosteric effectors.

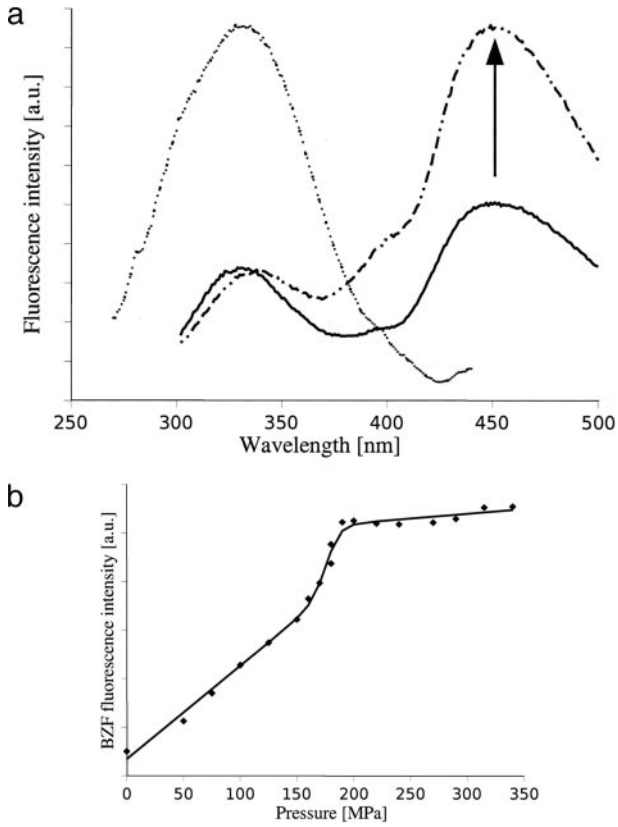

FIGURE 5. *a,* fluorescence emission (excited at 290 nm) and excitation (registered at 460 nm) spectra of oxy-Hb with BZF bound. *Solid line,* emission spectrum at ambient pressure; *dashed line,* emission spectrum at 125 MPa. *Arrow* shows the emission of bound BZF. *Dotted line,* excitation spectrum registered at 460 nm. *b,* BZF emission intensity excited at 290 nm and registered at 450 nm *versus* pressure. The *solid line,* sigmoid fit to the data, $p_{1/2}$ is 177 MPa. *a.u.*, arbitrary units.

The Fluorescence of BZF—We observed that BZF became fluorescent upon binding to HbA. Fig. 5 shows the excitation spectrum and the emission spectrum of BZF excited at 290 nm when bound to oxy-Hb. As seen from the comparison of the excitation and emission spectra, excitation of the Trps may lead to energy transfer to BZF. In Fig. 5*a*, a broad emission band around 450 nm represents the contribution of protein-bound BZF to the fluorescence emission. A decrease in the fluorescence emission signal at the Soret band (~420 nm) because of the absorption of the porphyrins can also be seen in the figure. The intensity of the BZF peak around 450 nm varied with pressure and

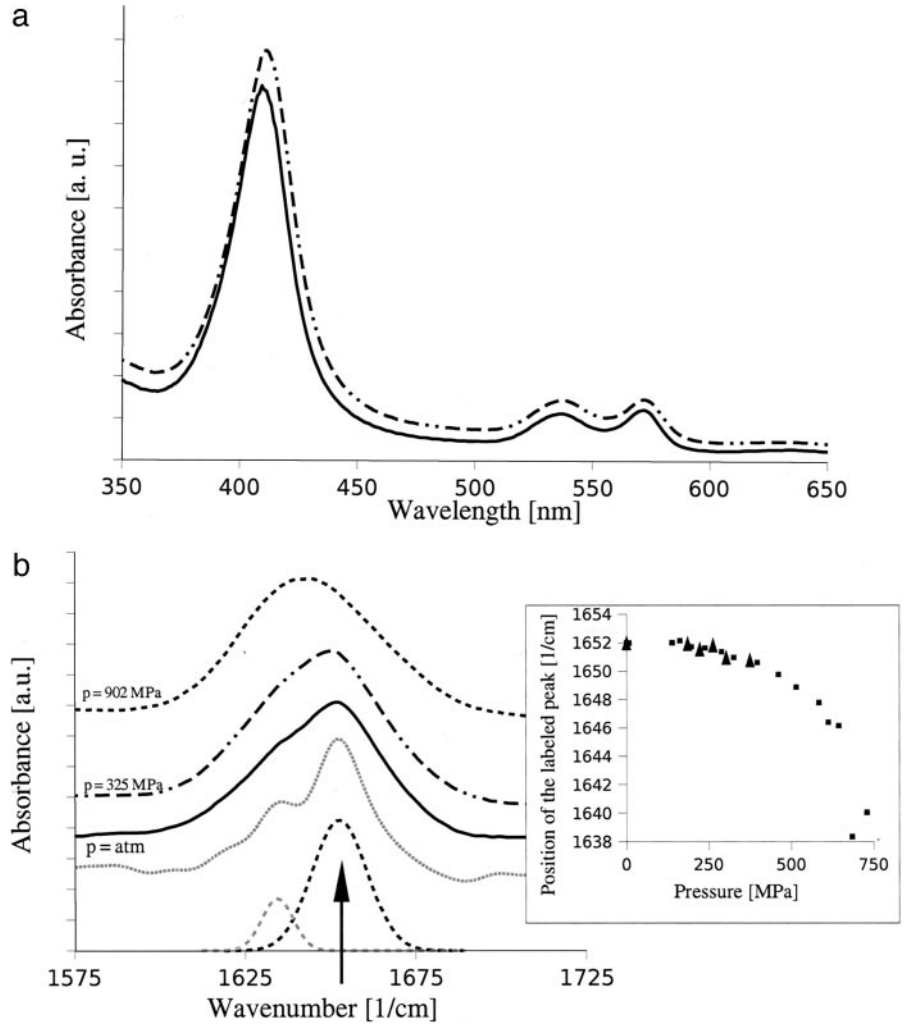

FIGURE 6. *a,* absorption spectrum of oxy-Hb measured in the pressure cell at ambient pressure (*solid line*) and at 350 MPa hydrostatic pressure (*dashed line*) at a concentration of 60 μM. Spectra are shifted along the *y-axis* relative to each other for clarity. Band maxima are around 420, 530, and 570 nm. *b,* FTIR spectra of oxy-Hb curves from the top are as follows: spectrum at 902 MPa (*dotted line*), 325 MPa (*dashed line*), at ambient pressure (*solid line*), deconvoluted spectrum at ambient pressure (*gray dotted line*), and gaussian decomposition of the amide-I band (*gray* and *black dotted curves*). An *arrow* indicates the gaussian characteristic for α-helical structure. *Inset* shows the maximum position of this band *versus* pressure for oxy-Hb (*squares*) and α-oxy-Fe-βZn-Hb (*triangles*), both in the stripped condition. *a.u.*, arbitrary units.

showed a sigmoidal character, as shown in Fig. 5*b*. Characteristic pressures obtained by fitting a sigmoid curve agreed well with the data from the emission maximum of the Trp signal. A linear increase superimposed on the sigmoid change can be observed before and after the transition. These were corrected in the fitting.

Optical Absorption and FTIR Spectroscopy to Assess Possible Unfolding Effects of High Pressure—As a control of sample quality, optical absorption spectra were recorded at ambient pressure and, in some cases, also at 250–350 MPa hydrostatic pressure. In the case of the stripped reference, samples of several absorption spectra were recorded from ambient pressure up to 350 MPa. No signs of denaturation, met-Hb formation, or deoxygenation were observed in these spectra. This was the case for both oxy-Hb and α-oxy-Fe-βZn-Hb stripped or with effectors. As an example, the absorption spectra of stripped oxy-Hb at ambient and at 350 MPa pressures are shown in Fig. 6*a*.

To further ensure the absence of any unfolding in this pressure range, we recorded FTIR spectra of oxy-Hb and α-oxy-Fe-βZn-Hb up to 902 MPa. Fig. 6*b* shows the FTIR spectra of oxy-Hb at ambient, 325 MPa, and 902 MPa pressures. In Fig. 6*b,* an *arrow* indicates the band characteristic for α-helical structure, best seen after deconvolution. The change of the position of this band is shown in Fig. 6*b, inset*. It is seen that the change is negligible in the 0.1–250-MPa pressure range used in our studies.

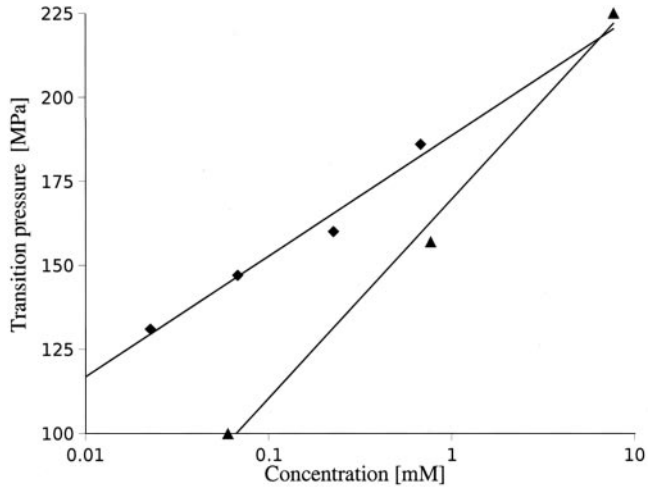

FIGURE 7. **Concentration dependence of $p_{1/2}$ values of α-oxy-Fe-βZn-Hb (*squares*) and of oxy-Hb (*triangles*).** *Continuous lines* are the fitted straight lines to the data.

Effect of Protein Concentration—The pressure stability measurements were performed at various protein concentrations in the stripped case. Table 1 summarizes the corresponding transition pressures, and in Fig. 7 we show the data for stripped oxy-Hb and α-oxy-Fe-βZn-Hb. The transition pressure strongly depends on the concentration of the protein in both quaternary states, with the concentration dependence being larger for oxy-Hb. The transition pressure *versus* the total protein concentration in a semi-logarithmic plot is linear as expected from the influence of concentration on a tetramer-dimer equilibrium.

DISCUSSION

Sensitivity of Trp Fluorescence to Pressure-induced Structural Changes at the Dimer-Dimer Interface—The HbA tetramer has 6 Trp residues, one in each α and two in each β subunits. It was

TABLE 2

Distance data of Trps to the hemes in the R- and T-state average structures after 2 ns molecular dynamics simulations

Inter- and intradimer distances are marked with bold font for β37 Trps.

Heme	Trp	HbR stripped	HbR + DPG	HbT stripped	HbT + DPG
α_1	$\alpha_1$14	16.68	16.40	16.57	19.17
α_1	$\beta_1$15	35.91	34.16	32.56	34.39
α_1	**$\beta_1$37**	**25.95**	**27.70**	**26.49**	**26.81**
α_1	$\alpha_2$14	35.21	37.69	39.79	39.30
α_1	**$\beta_2$15**	42.13	41.76	40.38	38.10
α_1	**$\beta_2$37**	**14.97**	**15.30**	**17.05**	**16.57**
β_1	$\alpha_1$14	33.88	35.36	34.51	36.13
β_1	$\beta_1$15	19.99	18.73	15.30	17.57
β_1	**$\beta_1$37**	**14.45**	**15.20**	**15.88**	**16.44**
β_1	$\alpha_2$14	40.27	40.59	43.50	41.69
β_1	$\beta_2$15	38.49	39.70	41.04	39.83
β_1	**$\beta_2$37**	**29.91**	**34.72**	**37.50**	**36.19**
α_2	$\alpha_1$14	36.75	39.61	38.87	41.65
α_2	$\beta_1$15	45.53	42.60	37.77	40.79
α_2	**$\beta_1$37**	**17.11**	**16.31**	**15.41**	**17.95**
α_2	$\alpha_2$14	16.68	16.51	18.19	16.76
α_2	$\beta_2$15	34.97	33.41	34.12	33.91
α_2	**$\beta_2$37**	**27.57**	**28.72**	**27.79**	**25.88**
β_2	$\alpha_1$14	40.68	40.41	41.23	44.40
β_2	$\beta_1$15	40.49	38.57	39.29	39.08
β_2	**$\beta_1$37**	**29.35**	**32.13**	**34.65**	**37.89**
β_2	$\alpha_2$14	34.06	34.00	36.22	36.55
β_2	$\beta_2$15	17.25	18.08	17.73	15.36
β_2	**$\beta_2$37**	**15.54**	**15.55**	**15.02**	**19.80**

realized some time ago that Trp fluorescence could be used to monitor conformational changes, *i.e.* T to R transition, and this sensitivity of the signal was assigned mostly to Trps-β37, which are located at the $\alpha_1\beta_2$ and $\alpha_2\beta_1$ subunit interfaces (31, 32). In resonance Raman spectra obtained by UV excitation, the contribution assigned to these Trp residues can be separately analyzed and used to monitor local structural changes in the interface region (see for *e.g.* Refs. 37 and 38). In a fluorescence study, the sensitivity of the signal to structural changes relies significantly on the conditions for quenching by Förster-type energy transfer to the hemes. The Trps in Hb are within short distances from one or more hemes of the structure; thus the distance requirements of energy transfer are fulfilled. Table 2 lists distance data for all Trps to the hemes obtained from average HbA structures after 2 ns of molecular dynamics, as described previously (48). The Trp-β37 is the Trp closest to the neighboring α subunit heme (Trp-$\beta_1$37 to the α_2 heme, and Trp-$\beta_2$37 to the α_1 heme). This distance is liable to become easily perturbed by changes at the interface. It should be noted, however, that Trp-$\alpha_1$14, Trp-$\beta_1$15, and Trp-$\beta_1$37 are within a short distance of their respective intrasubunit heme groups (the same holds for Trp-$\alpha_2$14, Trp-$\beta_2$15, and Trp-$\beta_2$37) and thus are also subject to energy transfer to this heme, but because this heme is part of their respective subunits, a possible dimer-dimer separation should not perturb this type of energy transfer significantly. Furthermore, Trps-α14 and -β15 are far away from the interface; a change at the interface region should not perturb their fluorescence properties significantly. Based on the distance data, one can suppose that the fluorescence of Trps-β37 will be sensitive to dimerization. The structural features (Trp heme distances are in the range sufficient for energy transfer) explain that the fluorescence of Zn-PP-IX can be excited through Trp excitation at 290 nm (see Fig. 1*b* and *inset*). Energy transfer could also be tracked down indirectly by the low quantum yield of Trp emission in HbA.

The Changes in Trp Fluorescence in the Studied Pressure Range Are Not Because of Local Conformational Changes, Unfolding, or Denaturation—Before reaching conclusions from our results concerning the tetramer-dimer equilibrium of R- and T-state HbA associated with allosteric effectors, we have to consider the possibility of other mechanisms having an effect on the Trp emission. Unfolding or denaturation under pressure could also cause changes in the Trp emission. We argue to rule out these possibilities, as follows:

a) The 100–200-MPa pressure range is very low compared with the typical pressures needed for protein unfolding. We have shown previously that myoglobin is pressure-stable up to 650 MPa (22, 49, 50). Our results presented in this paper also show no signs of denaturation in the pressure range up to 250 MPa, as can be seen in the *insets* of Fig. 2, Fig. 3, and Fig. 6*b*. Recently (51), a denaturation pressure of 400 MPa was reported for the isolated subunits of HbA; 100–200 MPa used in this study is significantly lower, and thus it is not reasonable to expect denaturation at this low level of pressure.

b) A second argument comes from the absorption spectrum at 350 MPa (see Fig. 6), where the Trp emission is already red-shifted with respect to the initial emission spectrum. No significant changes, except a slight red shift, can be seen in the Q-band and in the Soret region. Denaturation of the protein would be clearly seen in the absorption spectrum of the porphyrin, and absorption spectra recorded after releasing the pressure also show no signs of sample denaturation. Also, as observed in the Q-band region, no change in the spin state or in the coordination state of the heme occurs in the pressure range used. Adlen *et al.* (30) reported resonance Raman and optical absorption data in the function of pressure that they interpreted as resulting from changes in the spin state of the heme in oxy-Hb at 150 MPa and from further coordination changes at 350 MPa. Hamdane *et al.* (51) found that high pressure up to 700 MPa enhanced hexacoordination in globins. We observed neither of these effects in our samples within the studied pressure range. These reported effects could arise from different sample preparation methods, different pH values, or from different buffers used, which can all change the behavior of the sample under pressure.

The spectra shown in Fig. 6 differ in a small red shift of the Soret band around 420 nm. This effect is the same as shown in Fig. 4 and can be explained by the change of the electronic transition energy due to applying high pressure that decreases the distance between the chromophore and the interacting units (atomic groups). This change of the electronic transition energy is supposed to be proportional to the solvent shift at atmospheric pressure. If the interaction of the chromophore with the atomic groups of the protein matrix is dominated by one kind of interaction with a potential energy of $1/R^n$ distance dependence, one observes a linear shift of the transition energy as a function of pressure (52–54). We observed a linear red shift in both cases that has also been reported for other heme proteins (47, 49). The linear shift observed in the studied pressure range shows that

the structure of the heme pocket in general was not affected, and we only see an overall elastic effect.

c) It is well known that pressures of this range typically affect intermolecular interactions and cause the dissociation of oligomers (55). An earlier HbA fluorescence study (28) found reduced molecular volumes calculated from the fluorescence lifetime and anisotropy of a covalently attached fluorescent label 5-dimethylaminonaphthalene-1-sulfonyl under pressures up to 250 MPa. The authors interpreted these changes in terms of dissociation and not denaturation.

d) Besides conformational changes induced by pressure, we have to consider the possibility of deoxygenation because of pressure. This, however, would lead to almost a magnitude stronger shift of the Soret band (an almost 20 nm red shift of the Soret band would occur upon deoxygenation) than the shift observed. Thus, we can rule out pressure-induced deoxygenation in this pressure range.

e) FTIR spectroscopy does not show significant changes in the amide-I band position (characteristic for α-helical structure) up to 350 MPa, as can be seen in Fig. 6*b*. Because Hb is a predominantly α-helical structure, this rules out unfolding of any helices in this pressure range. To demonstrate pressure-induced unfolding, we present the FTIR spectrum acquired at 902 MPa, which clearly shows an unfolded state. This spectrum is, however, very different from the ones corresponding to the pressure range in our studies.

f) Myoglobin is a monomeric heme protein, and its tertiary structure closely resembles the structure of a HbA subunit. To model the effect of high pressure on a single HbA monomer, we acquired Trp emission spectra of myoglobin in the same pressure range as used in the HbA studies. This shows striking differences as follows: both the shift of the maximum position and the intensity change are strictly linear, as shown in Fig. 3*a* and Fig. 2*a*, respectively. It has been reported in the literature how pressure itself influences the fluorescence spectrum of Trp in Tris buffer, in the presence of alcohol or glycerol, and when it was incorporated in a small peptide (56). In all cases the authors observed a linear, continuous red shift induced by pressure. This effect, attributed to the increase of water density and dielectric constant under pressure, would cause a shift of 1–2 nm in the pressure range studied. The shift of the maximum position in our measurements is in this range, although somewhat larger, which can be attributed to the presence of the protein matrix. It is interesting to note that this red shift is comparable with the shift of the Soret peak and of the fluorescence maximum position of the Zn-porphyrin emission (*cf.* Fig. 4) of Hb, showing the presence of the same elastic compression in Hb. None of the transition-like features of Hb appear in the fluorescence of myoglobin. It should also be considered that an elastic compression, which shortens the heme-Trp distance, would itself decrease the intensity of the Trp fluorescence because of an increase in energy transfer. This latter effect is expected to occur also in Hb but is overwhelmed by another effect, which we attribute to pressure-induced dissociation of the tetramer.

The Pressure Effect on Trp Fluorescence Emission Shows Pressure-induced Dimerization—The emission spectrum of the Trps undergoes clear changes when the HbA samples are subjected to high pressure (Figs. 1 and 2). Because we ruled out pressure-induced unfolding, we present our argumentation for dimerization as follows.

a) A red shift of the Trp emission is usually assigned to a local environment of increasing polarity, as in the case of exposure to water (57, 58); however, changes in the electric field and in the dipole moments around the Trp residue can also result in the shift of the Trp emission spectrum (57). Because pressure-induced unfolding is very unlikely under our experimental conditions, this rules out significant electric field or dipole moment changes in Trp surroundings due to effects other than exposure to water. In the structure of HbA, two of the Trps, the Trps-β37, are located at the inter-subunit contact surface. These residues are somewhat buried in the tetramer but become solvent-exposed in the dimer form. Thus a tetramer-dimer transition and a consequent water exposure could explain the observed red shift.

b) Besides the red shift, the intensity of the fluorescence emission is increasing during the pressurization, in full agreement with the mentioned red shift of the emission maximum (Figs. 2 and 3). We attribute the increase of the Trp fluorescence intensity to a change in the efficiency of the energy transfer because of the tetramer dissociation. This effect would mostly influence Trps-β37, for these Trps the nearest extra subunit heme is the adjacent α-heme of the other dimer (*i.e.* α_2 heme for Trp-$\beta_1$37 and α_1 heme for Trp-$\beta_2$37). Published energy transfer rates (59) indicate that these Trps are the only ones having energy transfer rates to a heme in the adjacent dimer comparable with the heme in their own monomer (*cf.* Table 5 in Ref. 59). The known strong dependence of energy transfer efficiency on the donor-acceptor separation explains the significant quantum yield effect.

c) This argument is further supported by literature data, available for Trp fluorescence lifetimes of HbA (60). The ratio of a long component of the Trp lifetimes was shown to increase with pressure and was attributed to pressure-induced changes in the quaternary structure. In the case of the multimeric Hb of *Lumbricus terrestis*, a similar change in Trp fluorescence was also observed (61).

d) The concentration dependence of the transition pressure (Fig. 7) clearly supports the tetramer-dimer transition model. Dissociation reactions are known to depend strongly on the concentration of the initial molecule, whereas this dependence would not be expected for unfolding or denaturation reactions. Also, if the observed effect would be due to a possible shift in the ratio of possible different subpopulations in the T-state (see for *e.g.* Refs. 37–39), a concentration dependence would not be expected.

e) High pressure dissociates protein oligomers by squeezing water molecules into the voids. This model was experimentally verified by H/D exchange experiments (62). Theoretically, this is also expected because ordered water molecules have a smaller volume than those in the bulk solution, and thus based on the LeChatelier-Braun principle, the disintegration is favorable under increasing pressure. High pressure-induced dimerization and also monomerization of HbA have been demonstrated previously based on fluorescence labeling and anisotropy measurements (28). In our opinion, however, these data are not fully comparable with our results, because differences in the experimental condi-

TABLE 3

Dissociation constants and volume changes of Hb with various allosteric effectors

Type is the quaternary state, oxyHb or α-oxyFe-βZn-Hb, stripped to without allosteric effectors. Protein concentration was 60 μM in all cases. K_{d0} and ΔV values were calculated by fitting the model described in the text to the emission maximum position data. Uncertainty of the fitted values is typically 5%.

Type	Effector	K_{d0} (10^{-6} M)	ΔV
			ml/mol
Oxy-Hb	None (stripped)	1.41	−99.5
Oxy-Hb	100 mM Cl^-	1.22	−83.2
Oxy-Hb	2 mM IHP	0.47	−97.7
α-Oxy-Fe-βZn-Hb	None (stripped)	0.44	−105.3
α-Oxy-Fe-βZn-Hb	100 mM Cl^-	0.78	−106.6
α-Oxy-Fe-βZn-Hb	2 mM DPG	2.06	−103.6
α-Oxy-Fe-βZn-Hb	2 mM IHP	12.90	−83.4

tions (different buffers, pH values, and sample preparation methods) are known to influence the stability of the HbA tetramer. We used pH 7.4 where HbA is primarily in the tetrameric form. Also, there was no attempt reported to calculate dissociation constants from the data.

f) Besides the pressure-induced red shift and intensity increase in Trp fluorescence, we also observed a significant broadening in the Trp emission band. This we attribute to increased heterogeneity in the fluorescent Trps when dimerization took place. The broad Trp emission spectrum also reflects an initial heterogeneity of the fluorescent Trps, which can be partially attributed to the existence of conformational subpopulations (38). Our method is not able to resolve the contribution of these populations to the signal; however, each subpopulation is expected to be subject of dimerization. As we argued above, we feel confident that the major contribution to the change in the fluorescence signal under high pressure comes from the Trps-β37 and thus follows the studied effect.

Model to Extract Dissociation Constants from the Trp Fluorescence Changes—We suggest a simple model for the tetramer to dimer dissociation of HbA. We define a parameter α for the degree of dimer formation such that $\alpha = 0$ represents the fully tetrameric state and $\alpha = 1$ represents the fully dimeric state. Thus, $[T] = (1 - \alpha)C_0$ and $[D] = 2\alpha C_0$, where C_0 is the total protein concentration, and [T] and [D] are the tetramer and dimer concentrations (in mol/dm^3), respectively. The dissociation constant K_d can then be expressed as shown in Equation 1.

$$K_d = \frac{[D]^2}{[T]} = \frac{4\alpha^2 C_0}{1-\alpha} \qquad \text{(Eq. 1)}$$

Discarding the negative solution yields Equation 2,

$$\alpha = \frac{\sqrt{K_d^2 + 16 K_d C_0} - K_d}{8 C_0} \qquad \text{(Eq. 2)}$$

where K_d is a function of pressure as shown in Equation 3,

$$K_d = K_{d0} e^{\frac{-p \cdot \Delta V}{RT}} \qquad \text{(Eq. 3)}$$

and thus α is also a function of pressure. At ambient pressure, K_d is equal to the tetramer-dimer dissociation constant (K_{d0}) measured by conventional methods. Substituting Equation 3 into Equation 2 yields a sigmoid-like function for α, as shown in Equation 4.

$$\alpha = \frac{\sqrt{K_{d0}^2 e^{-2\frac{p\Delta V}{RT}} + 16 C_0 K_{d0} e^{\frac{-p\Delta V}{RT}}} - K_{d0} e^{\frac{-p\Delta V}{RT}}}{8 C_0} \qquad \text{(Eq. 4)}$$

We suppose that both the wavelength change of the Trp fluorescence maximum and that of the quantum yield of fluorescence are proportional to α. By choosing the maximum position of the Trp spectra, it can then be expressed as shown in Equation 5,

$$\lambda_{max} = \lambda_0 + \Delta\lambda \cdot \alpha \qquad \text{(Eq. 5)}$$

where λ_0 is the initial Trp emission maximum position corresponding to atmospheric pressure, and $\Delta\lambda$ is the shift in the maximum position corresponding to total dimerization. Substituting Equation 4 into Equation 5 yields Equation 6,

$$\lambda = \lambda_0 + \Delta\lambda \cdot \frac{\sqrt{K_{d0}^2 e^{-2\frac{p\Delta V}{RT}} + 16 C_0 K_{d0} e^{\frac{-p\Delta V}{RT}}} - K_{d0} e^{\frac{-p\Delta V}{RT}}}{8 C_0} \qquad \text{(Eq. 6)}$$

which can be directly fitted to the experimental data points and yield K_{d0} and ΔV parameters.

The $p_{½}$ (where $p_{½}$ indicates characteristic transition pressure at 50% transformation) values shown in Table 1 can also be expressed from the model, because they correspond to $\alpha = ½$. In this way we render typical pressure values to the studied cases (where C_0 is constant), when their K_d values are identical. The difference in $p_{½}$ means distinct K_{d0} parameters. Thus the data in Table 1 and Table 3 are characteristic for the same phenomenon (through Equation 3). The fitting procedure to yield $p_{½}$ from the data points, however, is less sensitive to the experimental error than the fitting of Equation 6 to obtain K_{d0} and ΔV. In the case of the complexes with BZF where the uncertainty of the data points was higher, we characterized the effect only by the $p_{½}$ values.

The data in Tables 1 and 3 show that the quaternary state (R or T) and the binding of allosteric effectors influence the tetramer-dimer dissociation constant in HbA. The effect of allosteric effectors is distinct in the R-state and in the T-state analogue.

Verifying the Validity of the Tetramer-Dimer Dissociation Model—A control of the model is to measure the concentration dependence of the phenomenon. Solving Equation 4 for α and substituting $\alpha = ½$ yields a logarithmic function of C_0 as shown in Equation 7.

$$p_{\alpha=\frac{1}{2}} = \frac{RT}{\Delta V} \cdot \log\left(\frac{K_0}{2 C_0}\right) \qquad \text{(Eq. 7)}$$

To validate our model, we conducted a concentration dependence study for both the R- and the T-analogue states in the stripped condition. We have observed a logarithmic dependence of $p_{½}$ on C_0 in both cases, as shown in Fig. 7, that supports our interpretation of pressure-induced dimerization. We note that the transition pressure changes only by

a few tens of MPa in our experiments, remaining in the range of 100 to 160 MPa, which is characteristic for subunit dissociation.

The tetramer-dimer transition interpretation is further supported by the fact that besides the Trp fluorescence signal, the BZF fluorescence intensity also showed a sigmoid change in accordance with the Trp signal. It was shown (12, 21) that BZF and similar derivatives bind primarily to the central cavity in HbA. This region is expected to be affected in a structural transition like dimerization. The increased quantum yield in this transition may originate from a structural change during dimerization, which makes new hydrophobic areas accessible to the already bound BZF molecules or for those in the solvent.

The Effect of Allosteric Effectors—A HbA solution is always a dynamic mixture of tetramers and dimers; however, the dimer concentration is usually very low. The dimer-tetramer equilibrium was extensively studied along with the kinetics of the dissociation (63–68). Under our conditions the dimer ratio is estimated to be less than 1% in the R-state and less than 0.1% in the T-state. Physiological conditions (high Hb concentration and close to neutral pH) shift the equilibrium toward the tetrameric form. Table 1 shows the characteristic $p_{½}$ values observed for the stripped samples and for the samples with Cl^-, IHP, and BZF, both in oxy-Hb and α-oxy-Fe-βZn-Hb samples. We also studied DPG binding to α-oxy-Fe-βZn-Hb. These data show a clear change in the $p_{½}$ values upon the binding of allosteric effectors and, consequently, also in the K_{d0} and ΔV values as listed in Table 3.

Considering the data for the R-state, the determined dissociation constants (K_{d0}) agree well with previous reports on R-state HbA (65), where tetramer to dimer dissociation constants were measured in the case of stripped human oxy-HbA and also in the case of the IHP-complexed HbA. A dissociation constant of 1 μM was found for the stripped case, which decreased to 0.18 μM when complexed to IHP. These results are in excellent correlation with our results shown in Table 3. In a study of the Bohr effect (65), the authors found a value of 0.5–7.9 μM for human oxy-HbA depending on the pH and protein concentration, which is again in good agreement with our results.

Compared with the R-state, in the case of the T-analogue we found an overall opposite effect: the allosteric effectors decreased the transition pressures as shown in Table 1. This trend points to an increase in the dissociation constant, as shown in Table 3. For deoxyhemoglobin, K_{d0} values 4–6 orders of magnitude lower than values for the R-state were reported in the literature (36, 65, 69). We also observed the same trend but the effect was smaller. This we attribute to the fact that we studied a T-state analogue, which, by having a more tense conformation (40), may be less sensitive to the binding of the effectors. This finding supports our choice of a semi-hybrid structure as a T-analogue and not a tetra-zinc-substituted Hb, which might be so tense that no effect could have been observed. To validate our K_{d0} values, it is useful to consider the $\Delta\Delta G$ value for the same two systems (oxy- and $\alpha(FeO)_2$-$\beta(Zn)_2$-Hb) found in Huang *et al.* (36). The ratio of the two tetramer to dimer dissociation constants derived from this value ($\Delta\Delta G$ = 0.2 kcal/mol) is ~0.7, which is very close to our experimental result. This good agreement we consider as an internal control of our method.

In the T-state analogue we could compare the efficiency of allosteric effectors of different chemical structures. DPG is structurally related to IHP; however, IHP is known to be a stronger effector in oxygen binding experiments (19). Our data show that DPG has the same kind of effect (increase of the dissociation constant) on the α-oxy-Fe-βZn-Hb than IHP but with less efficiency. This shows that difference in effector potency is manifested in the strength of interactions at the dimer interface. In a UV resonance Raman study where the Trp-β37–Asp-α94 H-bond strength could be monitored, no effect was observed when IHP was added to $\alpha(FeCO)_2$-$\beta(Zn)_2$-Hb in a proportion similar to our experiments (39). The resonance Raman study, however, monitors a local effect involving the Trps-β37, whereas in our study we report overall changes at the whole interdimeric interface. Thus the two findings cannot be directly connected. It would have been interesting to compare the effect of the phosphates with that of an aromatic molecule such as BZF. The intense fluorescence of this effector in the bound state, however, did not allow us to derive reliable dissociation constants for this complex. It can be seen in Fig. 5 that the fluorescence of BZF interferes with the Trp emission, making the evaluation of Trp emission maximum difficult, especially at high hydrostatic pressures, where the BZF emission outweighs the Trp emission signal. We can, however, conclude that changes in the BZF emission also indicate significant structural changes at the dimer interface in HbA. The effect of BZF seems to be different from that of DPG and IHP (see Table 1). In both R- and T-states BZF has a stabilizing effect on the interdimeric interface, in a way that the stability will be the same in the two states in the presence of BZF. This effect can be related to the results reported for an effector of similar structure, 2-[4-({[(3,5-dichlorophenyl)amino]-carbonyl}amino)phenoxy]-2-methylpropanoic acid, to cause the decrease of CO affinity when added together with IHP to $\alpha(FeCO)_2$-$\beta(Zn)_2$-Hb (39). The authors of this work attributed this affinity change to a conformational effect of the aromatic effector resulting in a more tense T conformation.

Changes in dissociation constants in the T-state analogue show that allosteric effectors induce conformational changes that propagate to the interface also in this form. It is interesting that changes caused by IHP or BZF binding were not observed in the heme pocket by resonance Raman spectroscopy in the fully deoxy-state of HbA (70). It can be that propagation of conformational changes from the interface to the heme pocket is inhibited in the entirely unligated state but not in partially or fully ligated states. The communication pathway from the interdimeric interface to the heme pockets is a topic of further detailed studies.

Until now we discussed the observed changes in the dissociation constants. It is also interesting to estimate how significant the direct effect of the change in K_{d0} may be on the oxygen association. This we can do for the R-state based on characteristic half-oxygen saturation (P_{50}) values from the literature (see for example Atha and Riggs (65), P_{50} = 0.4 mm Hg for the dimer form and 1.78 mm Hg for the tetramer). As an approximation,

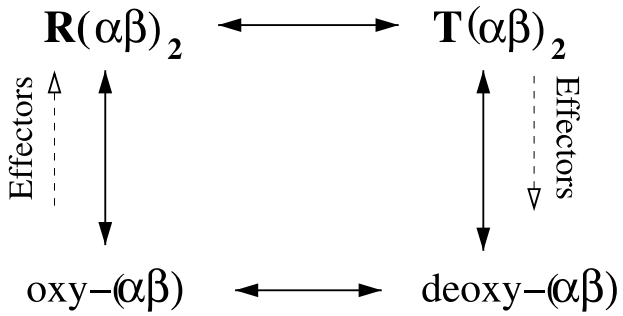

SCHEME 1. **Summary of the changes in equilibria caused by the binding of allosteric effectors.** *Double-ended arrows* indicate the various equilibria present in a HbA solution. *Dashed arrows* indicate the shifts in equilibria caused by the binding of allosteric effectors. *R*, R-state oxyhemoglobin (tetramer or dimer); *T*, T-state deoxyhemoglobin (tetramer or dimer).

we assume that the proportion of the dimers is low enough (less than 1%) such that the measured P_{50} values can be considered as a linear combination of the tetramer and dimer P_{50} values. From K_{d0} we know the proportion of the dimers, and so we can estimate the change in P_{50} caused only by a change in the tetramer-dimer equilibrium. Under our experimental conditions (*i.e.* 60 μM total HbA concentration) and for the IHP binding to oxy-Hb as an example, we obtain a 10% increase in P_{50} as an estimate. In the literature, the reported changes in P_{50} are more than a magnitude higher (18) as an effect of binding IHP, *i.e.* changes in the dissociation constants cannot account for the total effect of allosteric effectors on oxygen binding. However, there are cases, for instance that of the mutant Hb Howick, where dimerization plays a central role in the control of Hb function (71). In such a case, the changes in K_{d0} may have more significance. In the interpretation of the Bohr effect, the role of dimerization was also emphasized (65). We note, however, that in the T-state we can totally neglect the direct effect of K_{d0} on the P_{50} values, because K_{d0} is by orders of magnitude lower than in the R-state.

An overview of the effects of allosteric effectors on the tetramer-dimer equilibrium is presented in Scheme 1. *Double-ended arrows* in Scheme 1 represent the equilibrium, and *dashed arrows* show the influence of allosteric effectors. The changes in these equilibria are a direct consequence of tertiary structural changes propagating from the effector binding sites to the dimer interfaces in both quaternary states.

The volume changes during the dimerization process are also listed in Table 3. These changes arise from the following two factors: 1) from the change in the molecular volume of the protein, and 2) from the change in the volume of the water shell around the protein. In the oxy-Hb samples, volume changes do not correlate with the changes in dissociation constants and remain essentially the same in all cases. In the α-oxy-Fe-βZn-Hb samples, a 20% variation in the volume changes can be observed for the strong effector IHP. Further analysis of this effect may enable us to distinguish between the two factors contributing to this effect.

Conclusions—1) The good agreement with available data obtained by other techniques show that the dissociation constants for the tetramer to dimer transition of Hb determined by the pressure perturbation method yield reliable data. We note that among the possible techniques (*e.g.* size exclusion chromatography, light scattering, sedimentation velocity techniques, and CO binding experiments), the high pressure approach is outstanding in its simplicity.

2) The decrease in the dissociation constants upon binding of allosteric effectors in the R-state in itself leads to lower oxygen affinity. This direct effect, however, represents only a minor contribution to the reported change in oxygen affinity.

3) Allosteric effectors induce conformational changes in both the oxy-Hb and the α-oxy-Fe-βZn-Hb samples corresponding to the R- and T-states of HbA, respectively. These changes affect the structure of the interdimeric interface, resulting in changes of the dissociation constants. This finding supports the global allostery model by showing that conformational changes of the tertiary structure propagate from the effector binding site(s) to the interdimeric interfaces.

Acknowledgments—We appreciate the valuable discussions with Dr. M. Laberge and the critical reading of the manuscript and also for providing unpublished molecular dynamics data. We thank I. Kövesi for preparing Table 2 data from the 2-ns trajectory average HbA structures. We also thank Prof. Karel Heremans and Filip Meersman (Katholieke Universiteit, Leuven) for help with FTIR measurements.

REFERENCES

1. Perutz, M. F., Bolton, W., Diamond, R., and Murihead, H. (1964) *Nature* **203,** 687–690
2. Monod, J., Wyman, J., and Changeux, J. P. (1965) *J. Mol. Biol.* **12,** 88–118
3. Szabo, A., and Karplus, M. A. (1972) *J. Mol. Biol.* **72,** 163–197
4. Perutz, M. F. (1970) *Nature* **228,** 726–739
5. Baldwin, J., and Chothia, C. (1979) *J. Mol. Biol.* **129,** 175–220
6. Lalezari, I., Lalezari, P., Poyart, C., Marden, M., Kister, J., Bohn, B., Fermi, G., and Perutz, M. F. (1990) *Biochemistry* **29,** 1515–1523
7. Goodford, P. J., St-Louis, J., and Wootton, R. (1980) *Br. J. Pharmacol.* **68,** 741–748
8. Perutz, M. F., Fermi, G., Luisi, B., Shaanan, B., and Liddington, R. C. (1987) *Acc. Chem. Res.* **20,** 309–321
9. McLean, J. G., and Lewis, I. M. (1975) *Res. Vet. Sci.* **19,** 259–262
10. Arnone, A. (1972) *Nature* **237,** 146–149
11. Imai, K. (1982) *Allosteric Effects in Hemoglobin*, pp. 106–158, Cambridge University Press, Cambridge UK
12. Poyart, C., Marden, M. C., and Kister, J. (1994) *Methods Enzymol.* **232,** 496–513
13. Perutz, M. F., Wilkinson, A., Paoli, M., and Dodson, G. (1998) *Annu. Rev. Biophys. Biomol. Struct.* **27,** 1–34
14. Haire, R. N., and Hedlund, B. E. (1977) *Proc. Natl. Acad. Sci. U. S. A.* **74,** 4135–4138
15. Seixas, F. A., de Azevedo, W. F., Jr., and Colombo, M. F. (1999) *Acta Crystallogr. Sect. D. Biol. Crystallogr.* **55,** 1914–1916
16. Gray, R. D., and Gibson, Q. H. (1971) *J. Biol. Chem.* **249,** 4770–4775
17. Van Beek, G. G. M., and De Bruin, S. H. (1979) *Eur. J. Biochem.* **100,** 497–502
18. Yonetani, T., Park, S. I., Tsuneshige, A., Imai, K., and Kanaori, K. (2002) *J. Biol. Chem.* **277,** 34508–34520
19. Tsuneshige, A., Park, S., and Yonetani, T. (2002) *Biophys. Chem.* **98,** 49–63
20. Shibayama, N., Miura, S., Tame, J. R. H., Yonetani, T., and Park, S. Y. (2002) *J. Biol. Chem.* **277,** 38791–38796
21. Laberge, M., Kövesi, I., Yonetani, T., and Fidy, J. (2005) *FEBS Lett.* **579,** 627–632
22. Heremans, K., and Smeller, L. (1998) *Biochim. Biophys. Acta* **1386,** 353–370
23. Smeller, L. (2002) *Biochim. Biophys. Acta* **1595,** 11–29
24. Köhler, M., Friedrich, J., and Fidy, J. (1998) *Biochim. Biophys. Acta* **1386,**

255–289
25. Fidy, J., Balog, E., and Köhler, M. (1998) *Biochim. Biophys. Acta* **1386,** 289–305
26. Balny, C., Masson, P., and Heremans, K. (2002) *Biochim. Biophys. Acta* **1595,** 3–10
27. Silva, J. L., and Weber, G. (1993) *Annu. Rev. Phys. Chem. A.* **44,** 89–113
28. Pin, S., Royer, C. A., Gratton, E., Alpert, A., and Weber, G. (1990) *Biochemistry* **29,** 9194–9202
29. Ogunmola, G. B., Zipp, A., Chen, F., and Kauzmann, W. (1977) *Proc. Natl. Acad. Sci. U. S. A.* **74,** 1–4
30. Adlen, R. G., Satterlee, J. D., Mintorovitch, J., Constantinidis, I., Ondrias, M. R., Swanson, B. I. (1989) *J. Biol. Chem.* **264,** 1933–1940
31. Hirsh, R. E., and Nagel, R. L. (1981) *J. Biol. Chem.* **256,** 1080–1083
32. Hirsh, R. E., Zukin, R. S., and Nagel, R. L. (1980) *Biochem. Biophys. Res. Commun.* **93,** 432–439
33. Shibayama, N., Morimoto, H., and Kitagawa, T. (1986) *J. Mol. Biol.* **192,** 331–336
34. Stefano, Br., Stefano, Bu., Manfredini, M., Mozzarelli, A., Bolognesi, M., Deriu, D., Rosano, C., Tsuneshige, A., Yonetani, T., and Henry, E. R. (2000) *Protein Sci.* **9,** 683–692
35. Park, S. Y., Nagakawa, A., and Morimoto, H. (1996) *J. Mol. Biol.* **255,** 726–734
36. Huang, Y., Doyle, M. L., and Ackers, G. K. (1996) *Biophys. J.* **71,** 2094–2105
37. Samuni, U., Dantsker, D., Juszczak, L. J., Bettati, S., Ronda, L., Mozzarelli, A., and Friedman, J. M. (2004) *Biochemistry* **43,** 13674–13682
38. Samuni, U., Roche, C. J., Dantsker, D., Juszczak, L. J., and Friedman, J. M. (2006) *Biochemistry* **45,** 2820–2835
39. Samuni, U., Juszczak, L., Dantsker, D., Khan, I., Friedman, A. J., Pérez-González-de-Apodaca, J., Bruno, S., Hui, L. H., Colby, J. E., Karasik, E., Kwiatkowski, L. D., Mozzarelli, A., Noble, R., and Friedman, J. M. (2003) *Biochemistry* **42,** 8272–8288
40. Miyazaki, G., Morimoto, H., Yun, K. M., Park, S. Y., Nagakawa, A., Minagawa, H., and Shibayama, N. (1999) *J. Mol. Biol.* **292,** 1121–1136
41. Drabkin, D. L. (1946) *J. Biol. Chem.* **164,** 703–724
42. Berman, M., Benesch, R., and Benesch, R. E. (1971) *Arch. Biochem. Biophys.* **145**, 236–239
43. Tsuneshige, A., and Yonetani, T. (1994) *Methods Enzymol.* **231,** 215–222
44. Wong, P. T. T., and Moffat, D. J. (1989) *Appl. Spectrosc.* **43,** 1279–1281
45. Kauppinen, J. K., Moffat, D. J., Mantsch, H. H., and Cameron, D. G. (1981) *Appl. Spectrosc.* **35,** 271–276
46. Smeller, L., Goossens, K., and Heremans, K. (1995) *Appl. Spectrosc.* **49,** 1538–1542
47. Jung, C., Hui Bon Hoa, G., Davydov, D., Gill, E., and Heremans, K. (1995) *Eur. J. Biochem.* **233,** 600–606
48. Kövesi, I., Schay, G., Yonetani, T., Laberge, M., and Fidy, J. (2006) *Biochim. Biophys. Acta* **1764,** 516–521
49. Smeller, L., Goossens, K., and Heremans, K. (1996) in *High Pressure Science and Technology* (Trzeciakowski, W. A., ed) pp. 863–865, World Scientific Co. Pte. Ltd., Singapore
50. Meersman, F., Smeller, L., and Heremans, K. (2005) *Helv. Chim. Acta* **88,** 546–556
51. Hamdane, D., Kiger, L., Hui Bon Hoa, G., Dewild, S., Uzan, J., Burmester, Th., Hankeln, Th., Moens, L., and Marden, M. C. (2005) *J. Biol. Chem.* **280,** 36809–36814
52. Laird, J. J., and Skinner, J. L. (1989) *J. Chem. Phys.* **90,** 3274–3281
53. Zollfrank, J., Friedrich, J., Fidy, J., and Vanderkooi, J. M. (1991) *J. Chem. Phys.* **94,** 8600–8603
54. Zollfrank, J., Friedrich, J., Vanderkooi, J. M., and Fidy, J. (1991) *Biophys. J.* **59,** 305–312
55. Silva, J. L., Foguel, D., and Royer, C. A. (2001) *Trends Biochem. Sci.* **26,** 612–618
56. Ruan, K., Tian, S., Lange, R., and Balny, C. (2000) *Biochem. Biophys. Res. Commun.* **269,** 681–686
57. Reshetnyak, Ya. K., and Burnstein, E. A. (1997) *Biophysics* (*Engl. Trans. Biofizika)* **42,** 267–274
58. James, T. V., and Callis, P. R. (2001) *Biophys. J.* **80,** 2093–2109
59. Gryczynski, Z., Tenenholz, T., and Bucci, E. (1992) *Biophys. J.* **63,** 648–653
60. Gryczynski, Z., Beretta, S., Lubkowski, J., Razynska, A., Gryczynski, I., and Bucci, E. (1997) *Biophys. Chem.* **64,** 81–91
61. Hirsh, R. E., Vidugiris, G. J. A., Friedman, J. M., and Harrington, J. P. (1994) *Biochim. Biophys. Acta* **1205,** 248–251
62. Tanaka, N., Ikeda, C., Kanaori, K., Hiraga, K., Konno, T., and Kunugi, S. (2000) *Biochemistry* **39,** 12063–12068
63. Antonini, E., and Brunori, M. (1971) in *Hemoglobin and Myoglobin in Their Reactions with Ligands* (Neuberger, A., and Tatum., E. L., eds) pp. 110–112, Elsevier/North-Holland Biomedical Press, Amsterdam
64. White, S. (1976) *J. Biol. Chem.* **251,** 4763–4769
65. Atha, D. H., and Riggs, A. (1976) *J. Biol. Chem.* **251,** 5537–5543
66. Berjis, M., and Sharma, V. S. (1991) *Anal. Biochem.* **196,** 223–228
67. Chu, A. H., and Ackers, G. K. (1981) *J. Biol. Chem.* **256,** 1199–1205
68. Herskovits, T. T., and Ibanez, V. S. (1976) *Biochemistry* **15,** 5712–5721
69. Ackers, G. K., Johnson, M. L., and Mills, F. C. (1976) *Biochem. Biophys. Res. Commun.* **69,** 135–142
70. Coletta, M., Angeletti, M., Ascone, I., Boumis, G., Castellano, A. C., Dell'Ariccia, M., Longa, S. D., De Sanctis, G., Priori, A. M., Santucci, R., Feis, A., and Amiconi, G. (1999) *Biophys. J.* **76,** 1532–1536
71. Brittain, T. (1994) *Biochem. J.* **300,** 553–556